The Behavior of Joint Between Steel Beam and Concrete-Filled Steel Tube Column Under Fire

Ziyad Al-Gaboby [1]

Emad AH Al-Wesabi [2]

Ibrahim M. H. Al-Shaikh [3]

[1] Assistant Professor, Civil Engineering Department, Faculty of Engineering, University of Science and Technology, ziyad90@gmail.com

[2] Assistant Professor, Civil Engineering Department, Faculty of Engineering, University of Science and Technology, emadeng2011@gmail.com

[3] Assistant Professor, Civil Engineering Department, Faculty of Engineering, University of Science and Technology, ibraimalshaikh86@student.usm.my

https://doi.org/10.20428/JST.26.1.2

The Behavior of Joint Between Steel Beam and Concrete-Filled Steel Tube Column Under Fire

Abstract:

The results of a numerical study on the fire resistance of the joint between the steel beams, as well as the concrete-filled steel tube column (CFSTC) are provided utilizing the ABAQUS program. The analytical approach has been implemented, which comprises three steps of the sequential analysis, including fire analysis and heat transfer analysis, in addition to stress analysis for predicting the joint's behavior under a fire loading. They include models of the nonlinear 3D finite element of heat transfer, together with stress analysis. These illustrative models were validated by conducting a comparison between the data of the numerical output with the current experimental results in the literature. This test involves the reverse channel test, i.e., the joint's test against a fire. The conducted test is among different tests of fire; 10 tests that are available in the literature. The results showed good agreement when the numerical results were compared to the experimental results. Consequently, the models of the finite element can predict the joint's behavior under a fire loading.

Keywords: Finite element, ABAQUS, Concrete-filled steel tube, CFSTC, Steel tube, Fire, High temperatures, heat flux, Eurocode.

https://doi.org/10.20428/JST.26.1.2

سلوك مَفصل بين جسر معدني وعمود الأنبوب المعدني المملوء بالخرسانة تحت تأثير الحريق

الملخص:

يظهر هذا البحث نتائج دراسة محاكة حول مقاومة الحريق للمفصل بين الجسر المعدني وعمود الأنبوب المعدني المملوء بالخرسانة باستخدام برنامج ABAQUS. تم تنفيذ النهج التحليلي، والذي يتكون من ثلاث خطوات للتحليل المتسلسل، تحليل الحريق وتحليل انتقال الحرارة وتحليل الإجهاد للتنبؤ بسلوك المفصل تحت تأثير الحريق. وهي تشمل نماذج للعناصر المحددة الغير خطية وثلاثية الأبعاد لنقل الحرارة مع تحليل الإجهاد في آن واحد. تم التحقق من صحة هذه المحاكة من خلال إجراء مقارنة بين البيانات المستخرجة من المحاكة ونتائج اختبار تجريبي متوفر في الابحاث السابقة. يتضمن هذا الاختبار اختبار القناة العكسية، أي اختبار المفصل ضد الحريق. الاختبار الذي تم إجراؤه من بين اختبارات الحريق المختلفة (الاختبار العاشر). أظهرت النتائج توافق جيد عند مقارنة نتائج المحاكة بنتائج الاختبار التجريبي. وبالتالي، يمكن لنماذج العناصر المحددة أن تتنبأ بسلوك المفصل تحت تأثير الحريق.

الكلمات المفتاحية : العناصر المحددة؛ أنبوب معدني مملوء بالخرسانة؛ أنبوب معدني؛ حريق؛ درجات حرارة عالية؛ انتقال الحرارة؛ الكود الأوروبي.

1. Introduction

The CFSTCs were utilized amid the twentieth century, and most recently it has been popularly implemented in constructing bridges and high-rise buildings. This is because of its efficient structural performance. It exploited the combined effect advantage amid steel tube, as well as the concrete core working together. A steel tube can strict / restrict concrete, thereby increasing the compression strength, and simultaneously concrete inside the given steel tube can resist deformation with local buckling, enabling utilization of cross-sections that are thinner. Such composite sections can provide a sequence of features, including higher earthquake resistance, higher load-bearing capacity, thinner cross-section, more attractive appearance, faster construction technology, as well as more efficient fire resistance without the existence of external protection. Thus, the above-mentioned features potentially made CFSTCs a better alternative used by structural engineers and designers [1,2].

The CFSTCs can efficiently operate due to their higher fire resistance compared with hollow-steel columns' resistance. In many cases, they do not require any external side fire protection. When the steel tube is exposed to fire, it expands more rapidly than the compared concrete core and, therefore, it can carry a larger amount of an applied load. Thus, the heat flux can be transferred gradually from the given steel tube to concrete infill; the steel tube's rising temperature is moderately slow. This is because concrete infill can absorb heat from the wall of the steel tube, thereby reducing the steel tube's high temperatures. In the wake of a specified time of fire exposure (i.e., between 3020- min), the stiffness, as well as the strength of the steel tube started to rapidly decrease due to high temperature.

Consequently, the load has been transported gradually to concrete core. The steel tube currently functions as concrete protection only from the fire direct exposure, maintaining effective performance. By time, concrete strength started decreasing until failure occurred; this is because of compression strength or global buckling. Fig 1 shows this evolution regarding axial displacement, which has been measured at the column's top end with time [1].

https://doi.org/10.20428/JST.26.1.2

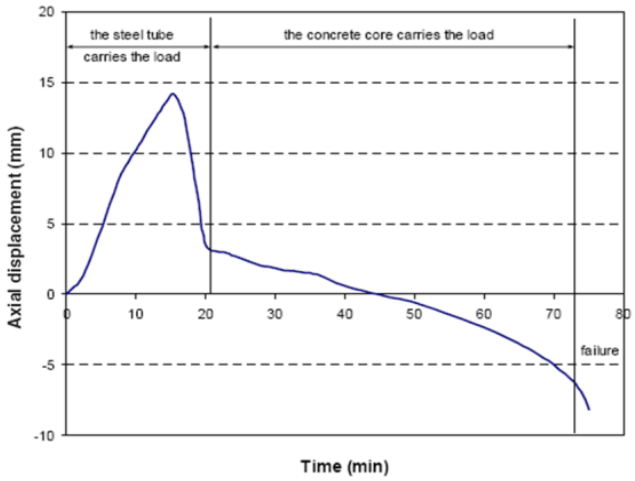

Figure 1: CFSTC's typical behavior subject to raised temperatures [1]

Joints are critical elements of any building structure and fire resistance is an important safety requirement in building design. However, although there have been extensive research studies about joint behavior at ambient temperatures [3,4] and member and frame structural behavior under fire conditions [5,6] that led to the development of the rational structural fire engineering design methods, a few studies were conducted about joint behavior in fire. Two factors might have contributed to the lack of studies about joint behavior in a fire, including the complexity of the investigated topic, as well as the simplistic treatment of joints in the design of fire resistance [3].

In previous studies, Elsawaf and Wang [7] conducted a numerical simulation using ABAQUS software to numerically model the behavior of joints between the steel beam and CFSTC under fire. Validation of the finite element model (FEM) was achieved by comparing the simulation and experimental results for the two fire tests studying cooling behavior. One of the tests used a fin plate connection and the other tests used a reverse channel connection. The FEMs give good agreement with the results of the tests.

This paper aims to validate the numerical output data, together with the obtained experimental results of the structural behavior utilizing failure modes, the development of deflections, in addition to the forces in beams.

2. Previous Experimental Studies

The experimental results of the test validated the obtained numerical results based on a previously conducted study because laboratories, which are

specialized in this field, are not available at university. In the test of the joint against fire, which has been carried out at the University of Manchester in the UK, a number of tests were conducted to examine ten varied types of joints according to [3]. Accordingly, test No. 10 (i.e., the Reverse Channel Test) was chosen to validate finite-element modeling's feasibility as the test results showed a potential to be advanced into a robust connection, which is characterized by strength, high stiffness, rotational capacity, as well as ductility.

The conducted tests of fire resistance were performed in the furnace, whereby Test No. 10 formed a frame that comprises 2 columns of 193.7×5mm concrete-filled tubes; the beam was 178×102×19UB of 1812mm length. Fig 2 shows that the beam has been connected to columns. The reverse channel section flanges 152×89 have been welded to the tube's wall. The 8mm- thickness endplate has been welded to the given beam on two sides, then bolted to the reverse channel using four (2 by 2) M20 grade 8.8 bolts, and no fire protection was detected on the given joints [3].

The relationships of the input temperature-time are shown in Fig 3 for the beam's flanges and the web, as well as steel tube, with connection zone, in addition to filled concrete. The average yield strength, the ultimate strength, together with the elastic modulus of steel members are listed in Table 1 at ambient temperatures utilized in the conducted experimental test. The average concrete cube strength recorded 46.2 MPa, whereas concrete density recorded 2305 kg/m^3.

At room temperature, the loads were gradually applied to the beam, and any obvious deformation was not observed at this stage in the specimen to avoid the steel beam's lateral torsion buckling before the occurrence of the beam's large deflection. After 23.1 minutes of fire ignition, the furnace has been turned off, and after 29.7 minutes of the conducted test, beam deflection began to slowly decrease. After 56 minutes, however, beam deflection began to slowly increase again. After 158 minutes, the door of the furnace was opened. After 320 minutes, the test has been completed without the frame's failure and fracture. The given loads were maintained successfully during the conducted test due to the absence of large deflection in the given steel beam [3].

https://doi.org/10.20428/JST.26.1.2

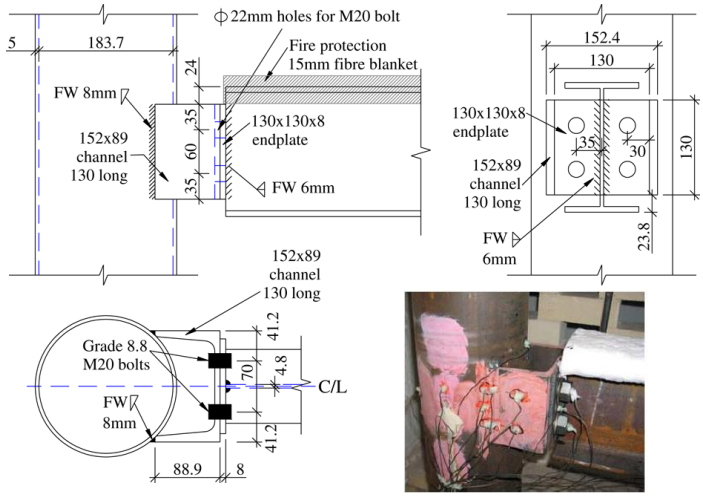

Figure 2: Geometrical details of the reverse channel connection [3]

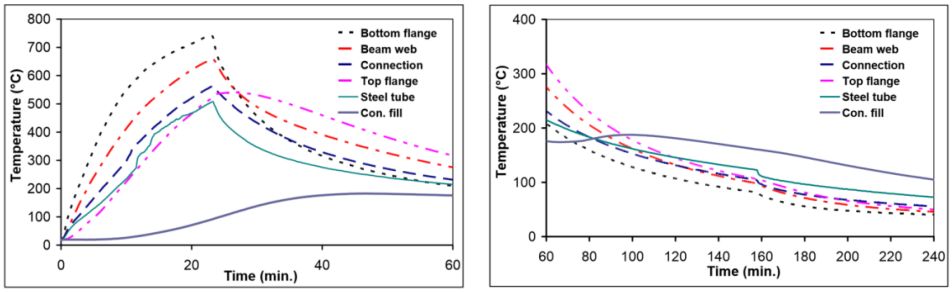

(a) Prior to 60 min. **(b) In the wake of 60 min.**

Figure 3: Time-temperature relationships [3]

Table 1: Mechanical property values of various steel members.

Component	Elastic modulus (MPa)	Yield strength (MPa)	Maximum strength (MPa)	Ultimate strain (%)
Beam Web	206606	352	493	32.1
Beam Flange	206378	309	477	34.9
Tubes	200001	406	539	29.5
End plate	200000	355	561	32.6
Reverse channel web	192280	397	562	27.1
Reverse channel flange	207811	351	561	32.6

3. Numerical Analysis

Many finite element programs (FEA) exist, which are capable of solving various simulations. These are utilized for conducting various analyses of static, heat transfer, dynamic, electrical response, and so on. Time, as well as cost tests, are also provided. The selected program, in this paper, is ABAQUS/Standard 6.12 as ABAQUS/Standard can provide automatic and direct user's control of time step, an extensive range of contact, as well as nonlinear materials' options, effective for analyzing the dynamic, static, electrical, and thermal response of linear, as well as non-linear models.

Moreover, three-dimensional numerical models were generated by means of the ABAQUS program for simulating the joint test (i.e., the reverse channel test) against fire based on the conducted experimental tests in [3]. The joint test (i.e., the reverse channel test) modeling in ABAQUS is shown in Fig 4.

The finite-element model is shown in Fig 5. Half of the given model was molded only as it is symmetric about the vertical axis through the beam's mid-span. The use of a given symmetry boundary condition at the beam's mid-span saves useful computation time; it also provides similar results regarding the full frames.

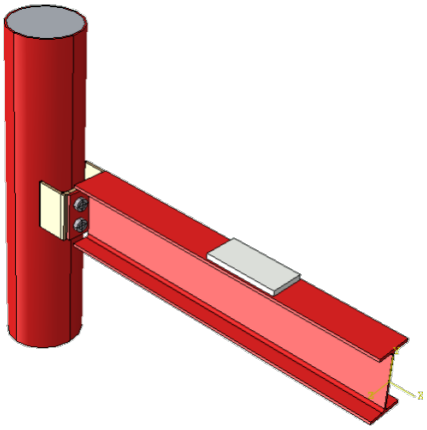

Figure 4: Modeling in ABAQUS of the joint (i.e., reverse channel) modeling

3.1 An Analytical Approach

Three-dimensional numerical models were created for simulating the track of the experimental tests. The track involves an analytical approach, which comprises 3 sequential analytical steps, including fire analysis and heat transfer analysis, as well as stress analysis.

https://doi.org/10.20428/JST.26.1.2

3.1.1 Fire Analysis

Many building codes designate a universally agreed temperature-time curve, being defined in ISO-834 Standard Fire [8] and characterized by gas temperature, which has continuously increased at a reduced rate with time. This curve is a standard pattern used in laboratories to test the structural element's resistance against fire; it does not mimic a real-life fire. The curve of the standard ISO 834, based on EC1 Part 12- Section 3.2.1[9], can be calculated by this Eq. as follows:

$$\theta_g = 20 + 345 \log 10(8t + 1) \quad (1)$$

, where θ_g refers to the temperature of the gas in the fire compartment [°C], t refers to time [min].

The ASTM El1915] 88-] (i.e., Standard Methods of Fire Tests of Building Construction and Materials) is the curve of the typical temperature-time, calculated by this approximated Eq. as follows:

$$\theta_g = 20 + 750[1 - \exp(-3.79533\sqrt{t})] + 170.1\sqrt{t} \quad (2)$$

, where θ_g refers to the temperature of the gas in the fire compartment [°C], t refers to time [hrs.].

Fig 5 shows two-nominal temperature-time curves.

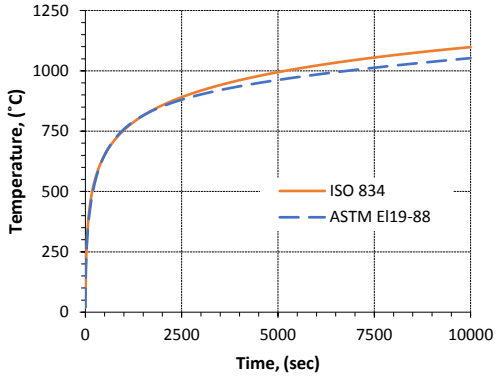

Figure 5: Different types of the fire curve [8]

3.1.2 Heat Transfer Analysis

The model of the heat transfer has been designed to achieve the distribution of the temperature at a given time during which the member's fire resistance is verified. Because the materials' thermal properties depend on heat transfer, the obtained results are extremely nonlinear [1].

The structural member's heat transfer is separated to two parts, including the first part, which is (net heat flux), i.e., heat transfer from a fire to the unprotected surface, where convective, as well as radiation heat transfer mechanisms, are combined. The second part involves conductive heat transfer in the given structural element, evaluated by using the heat conduction equation as shown in Fig 6.

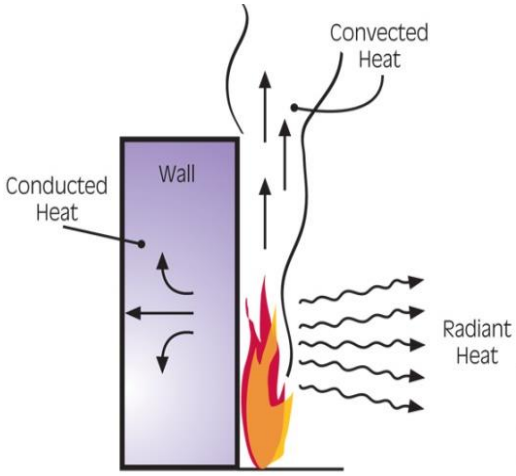

Figure 6: Structural member's heat transfer [1]

On the surfaces that are exposed to a fire, the given net heat flux (h_{net}), based on EC1 Part 12- Section 3, comprising convective heat flux ($h_{net,c}$), as well as radiation heat flux ($h_{net,r}$) as follows:

$$\dot{h}_{net} = \dot{h}_{net,c} + \dot{h}_{net,r}\ , (W/m^2) \qquad (3)$$

Convective heat transfer involves heat transfer between the places by the fluids' movement. The process, which is heat transfer by mass transfer, is in natural or free convection. The component of the net convective heat flux is determined by this equation:

$$\dot{h}_{net,c} = \alpha_C(\theta_g - \theta_m), (W/m^2) \qquad (4)$$

, where α_C refers to the heat transfer coefficient by equivalent convection to 25[W/m^2 K].

θ_g refers to the temperature of the gas in a vicinity of a fire unprotected member, [°C].

θ_m refers to the member's surface temperature, [°C].

https://doi.org/10.20428/JST.26.1.2

Radiation involves the energy transfer to a given body via absorption or emission of electromagnetic radiation. Thus, thermal radiation spreads through the given vacuum.

The net radiation heat flux $h_{net,r}$ can be determined by this equation:

$$h_{net,r}= \Phi\ \varepsilon_m\varepsilon_f\ \sigma[(\theta_r+273)^4-(\theta_m+273)^4],\ (W/m^2) \quad (5)$$

, where Φ refers to a configuration factor equivalent to 1, ε_m refers to the member's surface emissivity, which is equivalent to 0.7, ε_f refers to the fire emissivity, equivalent to 1, σ refers to the Stephan-Boltzmann constant, equivalent to $5.67\times(108\text{-})W/m^2$ K4, θ_m refers to the member's surface temperature [°C], and θ_r refers to the fire environment's effective radiation temperature [°C]

Conduction involves heat transfer from one given point to another point because of the difference in temperature. The given conductive heat transfer amid the contact surfaces can be identified by:

$$q = k\ (\theta_A\ -\ \theta_B\ ) \quad (6)$$

, where q refers to heat flux for each unit area that crosses an interface on one given surface from point A to point B on another, θ_A signifies the points' temperatures on the surfaces of the slave [°C], θ_B signifies the points' temperatures on master surfaces[°C], k refers to the conductance of the gap.

3.1.3 Stress Analysis

Nonlinear stress analysis has been performed simultaneously with the analysis of heat transfer so that the complete structural response is obtained (deformation, strain, and stress history) of the CFSTCs. Stress analysis has been performed via ABAQUS (2012) [10]. Structural analysis is obligatory to determine the column's fire resistance, in which, the previously computed temperature distributions, together with fire exposure time were taken as a starting point. The stress, as well as strain solution, were identified for each time step with the time, at which, the column's collapse occurred, under a specified applied load [1].

3.2 Material Parameters

The properties of the material and the stress-states were influenced by high temperatures. In this study, the mechanical properties of the high temperature were utilized as stated in Eurocode.

3.2.1 Thermal Properties

3.2.1.1 Concrete and Steel at High Temperatures

Eurocode 2 Part 1.2 (CEN 2004a) has been chosen in Section 3.3 [11], in addition to Eurocode 3 Part 1.2 (CEN 2005b) in Section 3.4 [12]. They describe the concrete and steel thermal properties at elevated temperatures, correspondingly. After the use of formulation of every thermal property of the concrete and steel based on Eurocode (2,3), a curve between the temperature and the thermal properties was drawn as shown in Figs 7 -15.

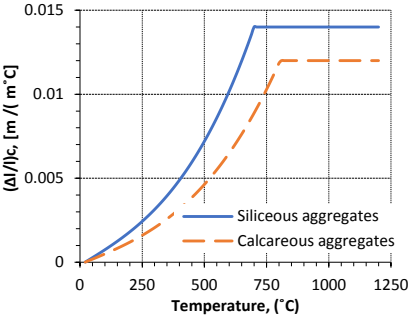

Figure 7: Thermal elongation of concrete at elevated temperatures based on EC2 Part 1-2 Section 3.3.1(1) [11]

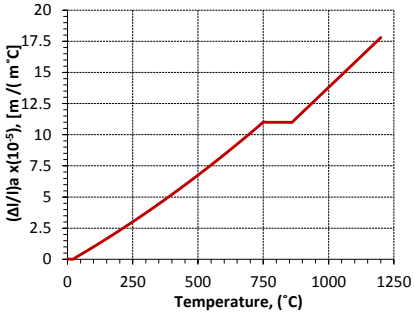

Figure 8: Steel thermal elongation at high temperatures based on EC3 Part 1-2 Section 3.4.1.1(1) [12]

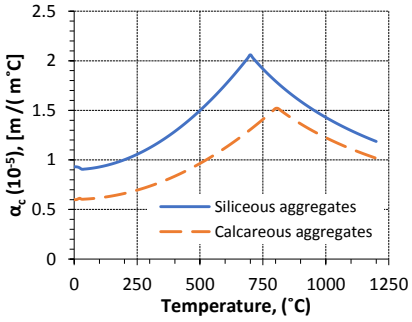

Figure 9: Concrete thermal expansion at elevated temperatures based on EC2 Part 1-2 Section 3.3.1(1) [11]

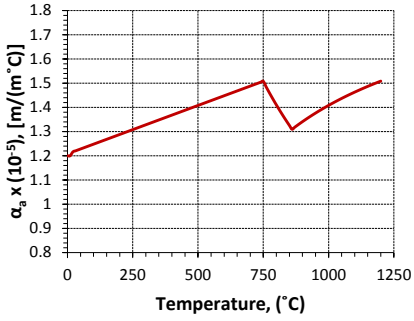

Figure 10: Steel thermal expansion at elevated temperatures based on EC3 Part 1-2 Section 3.4.1.2(1) [12]

https://doi.org/10.20428/JST.26.1.2

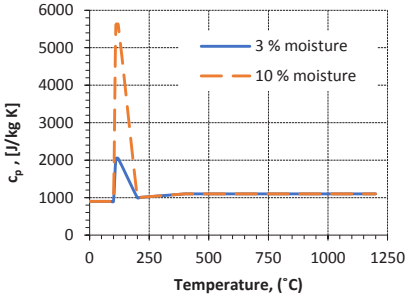

Figure 11: Concrete-specific heat at elevated temperatures based on EC2 Part 1-2 Section 3.3.1(1) [11]

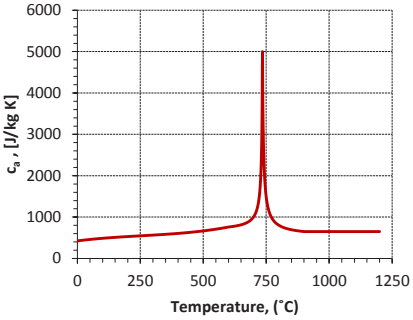

Figure 12: Steel-specific heat at elevated temperatures based on EC3 Part 1-2 Section 3.4.1.2(1) [12]

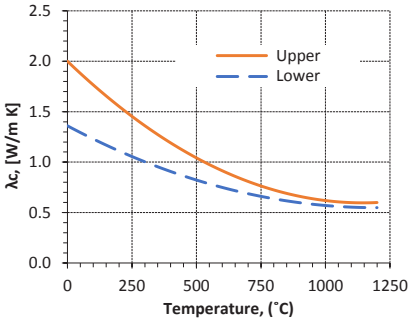

Figure 13: Concrete thermal conductivity at elevated temperatures based on EC2 Part 1-2 Section 3.3.3(2) [11]

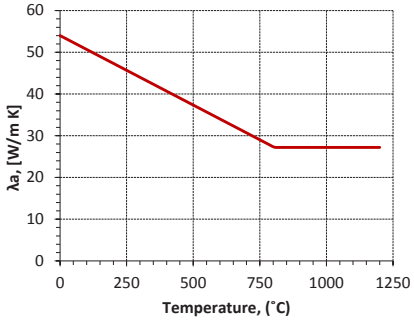

Figure: 14 Steel thermal conductivity at elevated temperatures based on EC3 Part 1-2 Section 3.4.1.3 (1) [12]

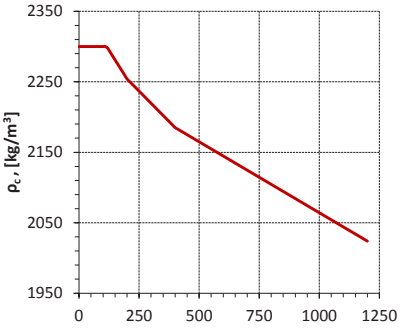

Figure 15: Concrete density at elevated temperatures based on EC2 Part 1-2 Section 3.3.2(3) [11]

3.2.2 Concrete Mechanical Properties at High Temperatures

3.2.2.1 Concrete at High Temperatures

These properties are the behavior of the concrete mechanical properties at elevated temperatures based on EC2 Part 1 -2 in Section 3.2.2.1[11]; taken from the given mechanical behavior from stress-strain relationships according to Fig 16, and is calculated using these equations:

Strain Range ($\varepsilon_{c,\theta}$) Stress($\sigma_{c,\theta}$)

$$\varepsilon_{c,\theta} \leq \varepsilon_{c1,\theta} \qquad \sigma_{c,\theta} = \frac{3\varepsilon_{c,\theta} \cdot f_{c,\theta}}{\varepsilon_{c1,\theta}\left[2 + \left(\frac{\varepsilon_{c,\theta}}{\varepsilon_{c1,\theta}}\right)\right]} \qquad (7)$$

$\varepsilon_{c1,\theta} \leq \varepsilon_{c\theta} \leq \varepsilon_{cu1,\theta}$ For a numerical purpose, the descending branch must be implemented. Linear models or non-linear models are allowed.

Two parameters define the equation models: compressive strength ($f_{c,\theta}$) of a specified temperature, strain ($\varepsilon_{c1,\theta}$) equivalent to ($f_{c,\theta}$). The parameters' values are achieved for every temperature via the application of reduction factors as illustrated in Table 3.1 of EC2 Part 12- in Section 3.2.2.1 according to Fig 17, including the ultimate strain value ($\varepsilon_{cu1,\theta}$). Regarding the given elastic part, the specified elastic modulus, as well as the Poisson's ratio have been determined, Poisson's ratio took a value equivalent to 0.2. Thus, the concrete elastic modulus has been computed at every temperature. As shown in Fig 18, the behavior of concrete (the stress-strain curve) at every temperature of a 31 MPa compressive strength of concrete.

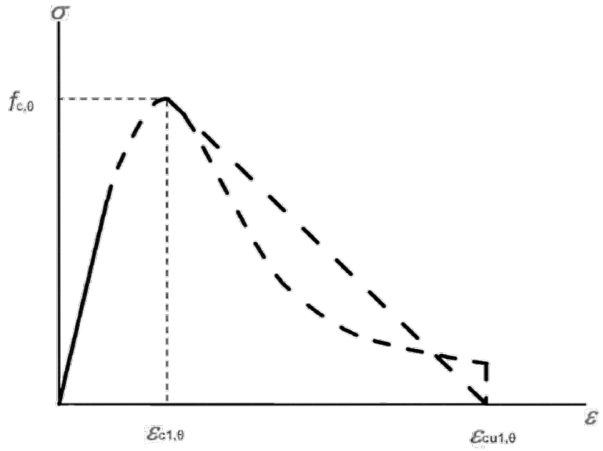

Figure 16: The mathematical model of concrete stress-strain relationships under compression at elevated temperatures [11]

https://doi.org/10.20428/JST.26.1.2

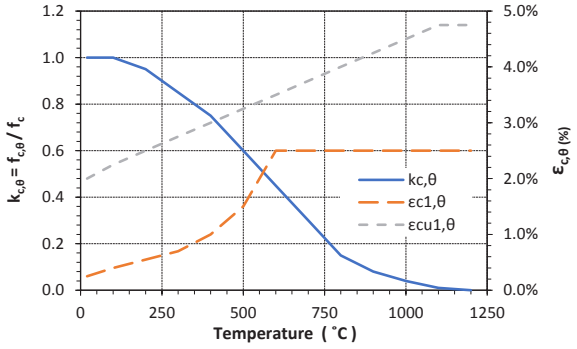

Figure 17: Reduction factors of concrete stress-strain relationships at elevated temperatures [11]

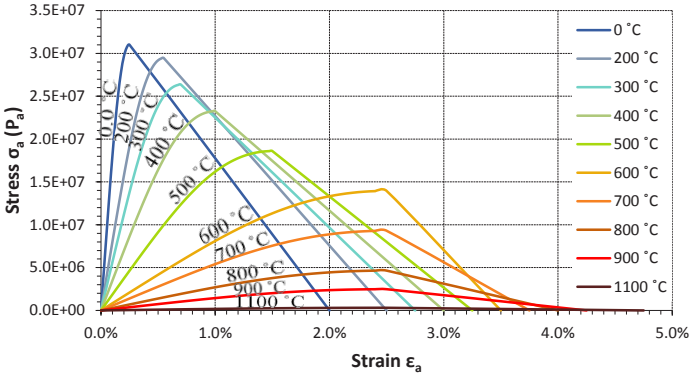

Figure 18: Curves of stress-strain at elevated temperatures of a 31 MPa concrete [11]

3.2.2.2 Steel Mechanical Properties at Elevated Temperatures

These properties represent the structural steel mechanical behavior at elevated temperatures based on EC3 Part 12- in Section 3.2.1(1,2) [12]. As shown in Fig 19, the overall stress-strain curve has been utilized to demonstrate resistances to compression or tension, and it is obtained based on these equations:

Strain Range (ε)	Stress ($\sigma_{c,\theta}$)	Tangent modulus	
$\varepsilon \le \varepsilon_{p,\theta}$	$\varepsilon E_{a,\theta}$	$E_{a,\theta}$	(8)
$\varepsilon_{p,\theta} < \varepsilon < \varepsilon_{y,\theta}$	$f_{p,\theta} - c + \left(\frac{b}{a}\right)\left[a^2 - (\varepsilon_{y,\theta} - \varepsilon)^2\right]^{0.5}$	$\frac{b(\varepsilon_{y,\theta} - \varepsilon)}{a\left[a^2 - (\varepsilon_{y,\theta} - \varepsilon)^2\right]^{0.5}}$	(9)
$\varepsilon_{y,\theta} \le \varepsilon \le \varepsilon_{t,\theta}$	$f_{y,\theta}$	0	(10)
$\varepsilon_{t,\theta} < \varepsilon < \varepsilon_{u,\theta}$	$f_{y,\theta}\left[1 - \frac{(\varepsilon - \varepsilon_{t,\theta})}{(\varepsilon_{u,\theta} - \varepsilon_{t,\theta})}\right]$	-	(11)
$\varepsilon = \varepsilon_{u,\theta}$	0.00	-	(12)

Parameters $\varepsilon_{p,\theta} = f_{p,\theta} / E_{a,\theta}$ $\varepsilon_{y,\theta} = 0.02$ $\varepsilon_{t,\theta} = 0.15$ $\varepsilon_{u,\theta} = 0.2$

Functions

$$a^2 = (\varepsilon_{y,\theta} - \varepsilon_{p,\theta})(\varepsilon_{y,\theta} - \varepsilon_{p,\theta} + c/E_{a,\theta})$$

$$b^2 = c(\varepsilon_{y,\theta} - \varepsilon_{p,\theta}) E_{a,\theta} + c^2$$

$$c = \frac{(f_{y,\theta} - f_{p,\theta})^2}{(\varepsilon_{y,\theta} - \varepsilon_{p,\theta}) E_{a,\theta} - 2(f_{y,\theta} - f_{p,\theta})}$$

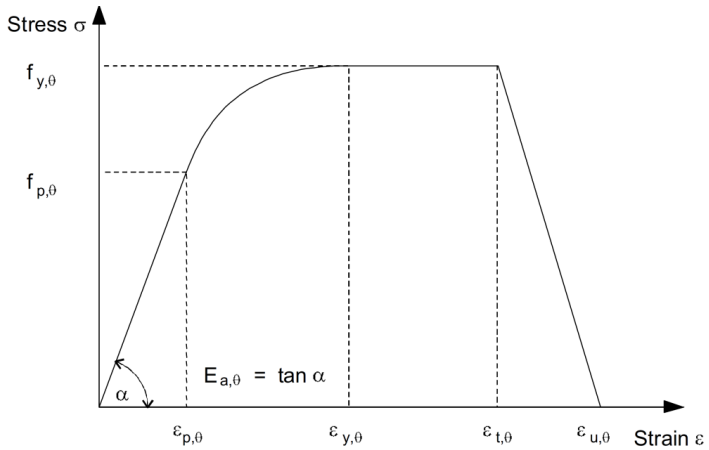

Fig 19: Stress-strain relationship of structural steel at elevated temperatures [12].

, whereby $f_{y,\theta}$ is the effective yield strength, and $f_{p,\theta}$ is the proportional limit, whereas $E_{a,\theta}$ refers to the linear elastic range slope, $\varepsilon_{p,\theta}$ refers to the strain at a proportional limit, and $\varepsilon_{y,\theta}$ is the yield strain, as well as $\varepsilon_{t,\theta}$ is the yield strength's limiting strain, in addition to $\varepsilon_{u,\theta}$ which refers to the ultimate strain.

https://doi.org/10.20428/JST.26.1.2

Table 3.1 in the EC3 Part 1 -2 in Section 3.2.1[12] illustrates these parameters' reduction factors f_y, f_p, and E_a of a given temperature. Fig 20 illustrates the variation for the reduction factors with the temperature.

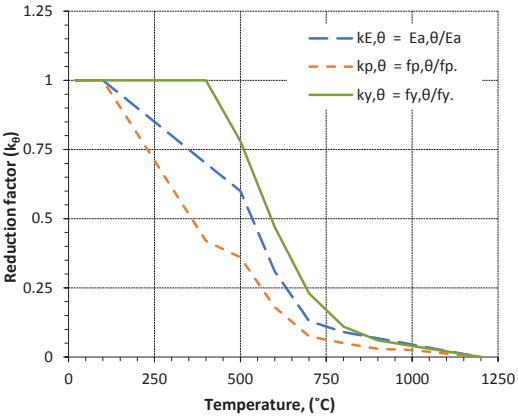

Figure 20: Reduction factors of stress-strain relationships of the structural steel at elevated temperatures [12]

Regarding the given elastic part, the specified elastic modulus, as well as the Poisson's ratio have been determined, where Poisson's ratio took a value equivalent to 0.3. Thus, the steel elastic modulus at elevated temperatures was taken based on Table 3.1 in the EC3 Part 1 -2 in Section 3.2.1[12]. The steel behavior (the stress-strain curve) at every temperature of tensile strength of 350 MPa is shown in Fig 21.

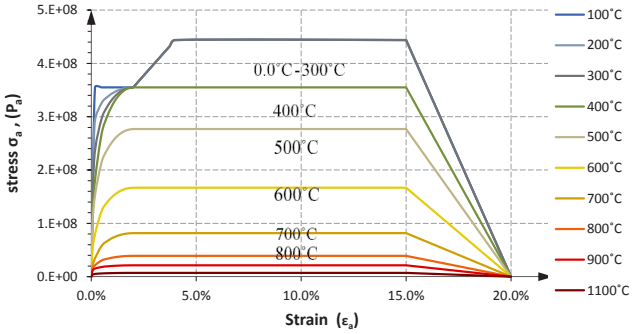

Figure 21: Curves of stress-strain at high temperatures of a350 MPa steel [12]

3.3 Element Types

The ABAQUS element library comprises many elements, whose names can be defined in a given set of specific symbols, each of these symbols performs a particular function. The elements' names, therefore, differ by changing

these symbols. In this study, the symbols in the implemented elements are described in Fig 22.

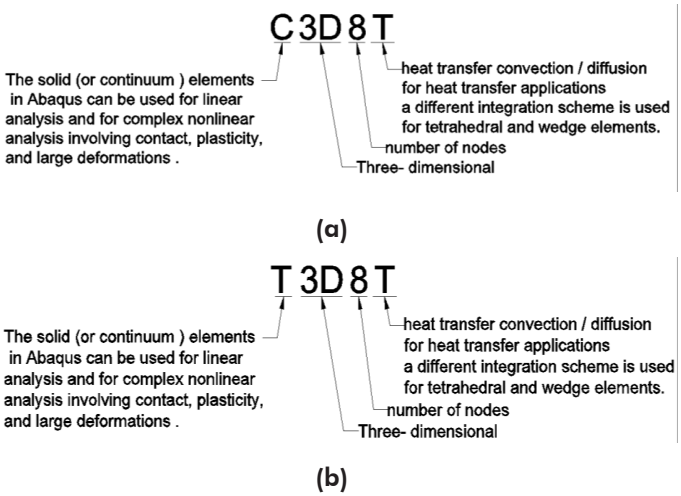

Figure 22: The description of the naming elements in ABAQUS, including (a) Solid elements (b)Truss elements.

For this work, three-dimensional solid elements (C3D8T) have been utilized for modeling steel tubes, concrete slabs, beams, concrete cores, bolts, as well as channel flanges. Three-dimensional solid elements (C3D6T) have been utilized for modeling the endplate of the beam and the channel's web. Moreover, three-dimensional truss elements (T3D2T) have been utilized for modeling the reinforcement of the rebar. Fig 23 demonstrates the way the model's different regions and parts have meshed.

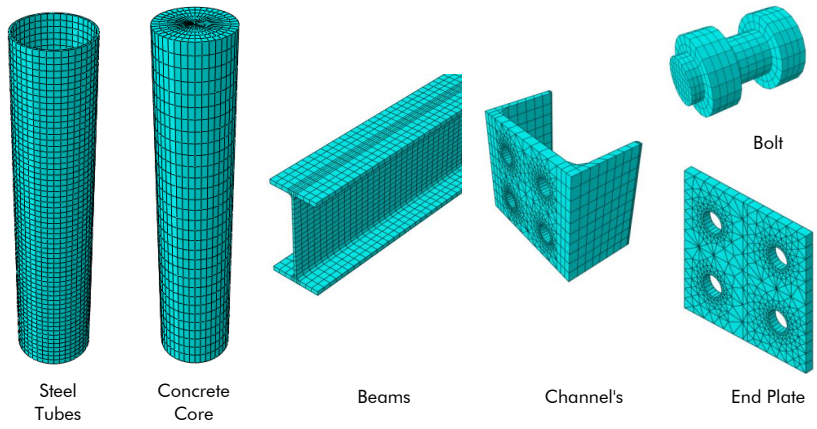

Figure: 23 Meshing of different regions and parts of the model

https://doi.org/10.20428/JST.26.1.2

3.4 Contact Constraints and Interactions

Several formulations of the constraint and interactions are provided by ABAQUS, and every contact (i.e., constraint and interactions) comprises numerous types. Only the implemented types in the study are described in this section.

3.4.1 Contact Interactions

Contact interactions that are on the three key factors depend on choosing a specific tracking approach, the contact discretization, along with assigning the roles of "master" and "slave" to contact surfaces [10]. Contact interactions were utilized in this study by selecting the main factors, i.e., the 'Small sliding', as well as the 'surface to surface' at the contact pair simulations in accordance with the ABAQUS manual recommendations for simulating the given contact interactions in between the steel tubes – the concrete cores, the Bolt head – the Web Channel, the Bolt Shank – the Bolt holes, the Nut – End Plate, as well as Web Channel – the End Plate.

3.4.2 Contact Constraints

There are many kinds of this type of contact, and one of these kinds was utilized in this study as described below:

3.4.2.1 Tie Constraint

Two surfaces are connected, and every node on the first surface slave has similar values of freedom degrees with the nearest point on the master surface. Regarding the surface elements, which are connected to the beam surface, offset distances in between the specified surface elements and the given beam are utilized in the constraints' definition, including the rotational degrees for the beam's freedom. A node-set can be specified as constrained; it contains the slave nodes irrespective of distance to the given master surface. Therefore, this kind is utilized in mechanical, and coupled temperature-displacement, or heat transfer simulations [10]. Tie constraint has been utilized in this study in between the concrete Slabs – the Beams, and the Steel Tubes – the Channel›s Flanges.

3.5 Properties of Contact

There are many properties of contact. The selected contact's thermal and mechanical properties are described as follows:

3.5.1 Mechanical Contact Properties

Mechanical interaction in between the contact surfaces' parts has been modeled with the use of two factors: 1) The normal behavior was implemented as the formulation of the hard contact. The hard contact's relationship with the contact pressure has been transmitted among contact surfaces, without any penetration of a slave surface onto a master surface at constraint locations, where any pressure value transfer is allowed when surfaces are in contact [10]. 2) The tangential behavior, including a specific friction model as one part of the surface. Therefore, the Coulomb friction model has been utilized with 0.3 as a constant friction coefficient [1,14,15].

3.5.2 Thermal contact properties

In the implemented numerical model, thermal interaction at the parts' surfaces, showing thermal resistance at the border between these parts were considered. ABAQUS permits heat flow crosswise the interface by using radiation or conduction. Both heat transfer modes are, generally, present to a limited degree. Based on the sensitivity analysis results, the constant value of 200 W/m2 K gap conductance at the border between the given steel tube and the concrete core was recorded, whereas 2000 W/m2 K gap conductance was recorded at the border between the steel parts [1].

4. Model Validation

ABAQUS program has been implemented to produce the FEM. The model accuracy is evaluated in this section by comparing the results obtained from the finite element analysis with the results obtained from the laboratory fire tests.

4.1 Test of Joint Against Fire

The model of three-dimensional numerical has been advanced by the ABAQUS program. The test in its second stage was corroborated by comparing the obtained results with the experimental results of the fire resistance test for the joint against fire based on the literature. Moreover, the utilized joint specimen in the validation stage has been tested at the University of Manchester in the UK. The joint characteristics were similar to [3]. Fig 24 displays the conducted comparison between the obtained numerical results versus emerging experimental results of a deformation model of the beam and joint, with a fire test picture. Accordingly, no failure has been observed in the given test specimen, as well as the numerical model. Fig 25 demonstrates

https://doi.org/10.20428/JST.26.1.2

a good comparison regarding the numerical and experimental displacement by the temperature. This is in agreement with the finding of Y.C. Wang (2013).

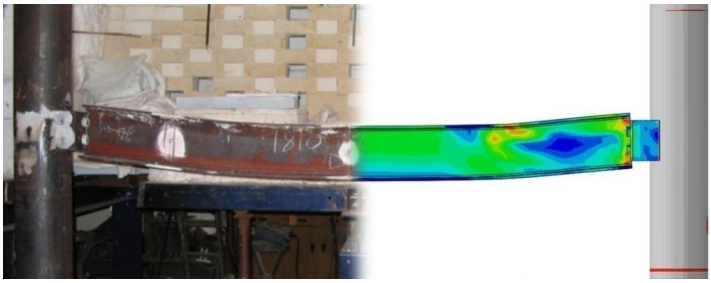

Figure 24: Comparison between the numerical and the experimental shape in the restrained beam by reverse channel connection (Test 10) [3]

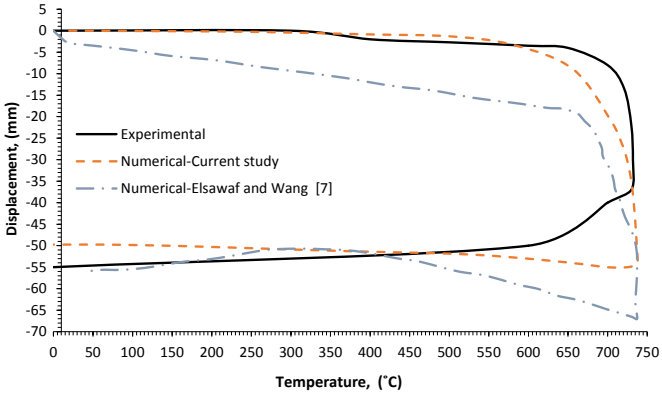

Figure 25: Comparison between the numerical-Elsawaf and Wang [7], numerical-current study and the experimental results of the mid-span deflection in the restrained beam by reverse channel connection [3]

5. Summary and Conclusion

The results of the conducted numerical study regarding fire resistance of the joints between the steel beams and the CFSTC are provided in this paper, utilizing the ABAQUS program to validate the numerical simulation model throughout the given cooling stage. Based on the results, good agreement has been observed for the obtained experimental results, as well as the vertical deflection–temperature relationships of beam and frames' final deformed shapes. Consequently, FEMs can predict the joints' behavior exposed to fire loads (the teat of the reverse channel). Also, Eurocode has been implemented to calculate the variables, which yielded good results regarding the CFST columns fire resistance compared to the results of the experimental fire tests. Further studies can investigate a multi-floor frame so that the frame behavior is analyzed with similar joints.

6. References

[1] Capilla, A. E. (2012). Numerical analysis of the fire resistance of circular and elliptical slender concrete filled tubular columns (Doctoral dissertation, Universitat Politècnica de València).

[2] Kodur, V. K. R., & Lie, T. T. (1995). Experimental studies on the fire resistance of circular hollow steel columns filled with steel-fibre-reinforced concrete. National Research Council Canada, Institute for Research in Construction.

[3] Ding, J., & Wang, Y. C. (2007). Experimental study of structural fire behaviour of steel beam to concrete filled tubular column assemblies with different types of joints. Engineering Structures, 29(12), 3485- 3502.

[4] Nethercot, D. A., & Zandonini, R. (1989). Methods of prediction of joints behaviour: beam-to-column connections, Structural Connection: stability and strength, edited by Narayanan, R.

[5] Wang, Y. C. (Ed.). (2002). Steel and composite structures: behaviour and design for fire safety. CRC Press.

[6] Wang, Y. C. (2005). Performance of steel–concrete composite structures in fire. Progress in Structural Engineering and Materials, 7(2), 86- 102.

[7] Elsawaf, S., & Wang, Y. C. (2013). Behaviour of restrained structural subassemblies of steel beam to CFT column in fire during cooling stage. Engineering structures, 46, 471 -492.

[8] ISO 834. (1980). International Standards Organization, Fire resistance tests, elements

of building construction, Switzerland.

[9] Eurocode 1 (EC1), (2002) Actions on Structures, Part 1.2: General Actions - Actions on Structures Exposed to Fire. Brussels, Belgium: Comité Européen De Normalisation.

[10] ABAQUS (2012) ABAQUS/Standard Version 6.12 User's Manual: Volumes I-III.

[11] Eurocode 2 (EC2), (2004) Design of Concrete Structures, Part 1.2: General Rules Structural Fire Design, Brussels, Belgium: Comité Européen De Normalisation.

[12] Eurocode 3 (EC3), (2005) Design of Steel Structures, Part 1.2: General Rules Structural Fire Design, Brussels, Belgium: Comité Européen De Normalisation.

[13] Iqbal, N. (2013) Restrained Behaviour of Beams in a Steel Frame Exposed to Fire, Luleå University of Technology.

https://doi.org/10.20428/JST.26.1.2

[14] Ali, M. M., Al-Wesabi, E., Al-Gaboby, Z., & Falah, N. (2014). NUMERICAL ANALYSIS OF MISSILE IMPACTS ON REINFORCED CONCRETE SLABS. Journal of science and Technology, 19(1).

[15] Alshaikh, I. M., Bakar, B. A., Alwesabi, E. A., Zeyad, A. M., & Magbool, H. M. (2021, October). Finite element analysis and experimental validation of progressive collapse of reinforced rubberized concrete frame. In Structures (Vol. 33, pp. 2361- 2373). Elsevier.